Table 3 (*cont.*)

N(1)–Cr—N(4)	82·7	N(2)–C(1)—C(2)	106·7	C(14)–C(13)–C(18)	119·1
N(2)–Cr—N(3)	80·3	N(3)–C(2)—C(1)	110·1	N(2)—I——N(4)	46·08
N(2)–Cr—N(4)	88·6	N(3)–C(3)—C(4)	123·8	C(1)—N(2)—I	95·8
N(3)–Cr—N(4)	96·0	N(4)–C(10)–C(11)	107·9	N(1)—C(11)–I	89·6
Cr—O(1)–C(18)	130·4	C(3)–C(4)—C(9)	123·8 (2·5)	Cr——I——N(4)	24·0
Cr—O(2)–C(9)	129·0	C(4)–C(5)—C(6)	121·2	Cr——I——N(2)	24·3
Cr—N(1)–C(11)	108·8	C(4)–C(9)—C(8)	118·7		
Cr—N(1)–C(12)	127·0	C(5)–C(6)—C(7)	116·8		
		C(5)–C(4)—C(9)	120·1		

Bond distances and angles involving the chromium and the iodine atoms are given in Table 3. The close approaches of N(2) and N(4) to the iodide anion could be taken to indicate hydrogen bonding and these may contribute to the apparent lengthening of the Cr–N(2) and Cr–N(4) bonds compared with the Cr–N(1) and Cr–N(3) bonds.

This work forms part of a project supported by a grant from the Australian Research Grants Committee. We thank Mr S. A. Mason for assistance with some of the computer programs, and Dr P. Leverett for Fig. 1.

References

BAKER, E. N., HALL, O. & WATERS, T. N. (1966). *J. Chem. Soc.* (*A*), p. 680.

BRAUN, R. L. & LINGAFELTER, E. C. (1966). *Acta Cryst.* **21**, 546.

BUSING, W. R., MARTIN, K. D. & LEVY, H. A. (1964) *ORFFE, A Fortran Crystallographic Function and Error Program*, ORNL-TM-306, Oak Ridge National Laboratory, Oak Ridge, Tennessee.

CRUICKSHANK, D. W. J. (1952). *Acta Cryst.* **5**, 511.

FREEMAN, A. J. (1959). *Acta Cryst.* **12**, 261.

FRASSON, E., PANATTONI, C. & SACCONI, L. (1964). *Acta Cryst.* **17**, 477.

GERLOCH, M. M. & MABBS, F. E. (1967). *J. Chem. Soc.* (*A*), p. 1598.

LINGAFELTER, E. C. & BRAUN, R. L. (1966). *J. Amer. Chem. Soc.* **88**, 2951.

O'CONNOR, M. J. (1966). Ph. D. Thesis, Monash Univ.

O'CONNOR, M. J. & WEST, B. O. (1968). *Austral. J. Chem.* **21**, 369.

WEI, L., STOGSDILL, R. M. & LINGAFELTER, E. C. (1964). *Acta Cryst.* **17**, 1058.

Acta Cryst. (1971). B**27**, 1509

Nuclear Magnetic Resonance Investigation of Fluoride Ions in Hydroxyapatite

BY W. VAN DER LUGT, D. I. M. KNOTTNERUS AND W. G. PERDOK

Solid State Physics Laboratory, University of Groningen, Melkweg 1, *Groningen, The Netherlands*

(*Received* 9 *February* 1970)

The position of fluoride minorities in hydroxyapatite [$Ca_5OH(PO_4)_3$] has been investigated by nuclear magnetic resonance methods. There is experimental evidence for the existence of OH–F–vacancy and OH–F–HO configurations parallel to the *c* axis. The internuclear distances permit the formation of weak OH···F hydrogen bonds. A discussion of the energy-level system for a linear array of two protons and a fluorine nucleus, coupled by dipolar interaction, is included.

Introduction

Fluorapatite [$Ca_5F(PO_4)_3$] and hydroxyapatite [$Ca_5OH(PO_4)_3$] are nearly isomorphous. Detailed descriptions of the structural aspects of apatites can be found in review articles by Young & Elliott (1966) and by Elliott (1969). Of the two compounds, fluorapatite is the more stable and, consequently, most mineral samples of hydroxyapatite contain some fluoride.

The space group attributed to fluorapatite is $P6_3/m$ (Hentschel, 1923; Náray-Szabó, 1930; Mehmel, 1930). According to Young & Elliott (1966) the lattice constants *a* and *c* are 9·364 and 6·879 Å respectively; slightly different values are mentioned by de Boer (1957), and in *Structure Reports* (1952, 1953, 1956). According to Náray-Szabó (1930) a fluoride ion in fluorapatite is situated at the intersection of a 6_3-axis and a mirror plane, exactly at the centre of a triangle of Ca^{2+} ions. The fluoride ions form linear chains along the 6_3-axis, the F–F distance being 3·44 Å.

The unit-cell dimensions of hydroxyapatite differ only slightly from those of fluorapatite. Kay, Young & Posner (1964) found $a=9{\cdot}422$ and $c=6{\cdot}883$ Å, and Bhatnagar (1969) $a=9{\cdot}4192$ and $c=6{\cdot}8867$ Å; see also *Structure Reports* (1952, 1953). For a hydroxyl ion, the

location at the intersection of a 6_3-axis and a mirror plane is, of course, incompatible with its symmetry. On the other hand, the neutron diffraction data cannot be explained without the assumption of a statistical mirror plane being present. Kay, Young & Posner (1964) have shown that the hydroxyl ions in hydroxyapatite also form linear chains along the 6_3-axis, but they are slightly displaced (0·37 Å) from the plane through the Ca^{2+} triangle. Consequently the mirror planes appear to be locally disturbed. The experimental data leave two possibilities for the orientation of the hydroxyl ions: they can point 'upward' or 'downward' along the *c* axis. Kay, Young & Posner propose two models for the distribution of the two orientations of the hydroxyl groups. In the 'ordered column' perfect translation symmetry exists in one and the same column, but the two orientations are distributed equally over the different columns. More realistic is the 'disordered column' model, which allows reversals to take place within one column. A simple geometrical consideration accounting for the dimensions of the OH^- group shows that for the disordered column model one needs some type of lattice defect in the chains to accommodate such reversals. The apatite lattice is known to be flexible enough to incorporate many types of impurities and defects. Kay, Young & Posner (1964) propose fluorine as an agent for producing reversals in a column.

Hydroxyapatite is an important biological material. It forms an important part of human bone and is the main constituent of dental enamel. It is well known that the administration of small amounts of fluoride reduces considerably the occurrence of dental *caries*. We expected that a determination of the position of fluorine ions in fluoride-contaminated hydroxyapatite should contribute to our knowledge of the mechanism of these biological effects of fluoride. Meanwhile, such a mechanism has been described by Young, Van der Lugt & Elliott (1969).

The above-mentioned considerations show that an important role is attributed to minorities of fluorine ions in stabilizing the hydroxyapatite lattice. Therefore a closer examination of its crystallographic position seemed appropriate.

Nuclear magnetic resonance work on apatites has been reported by Hayashi (1960), Myers (1965*a*, *b*), van der Lugt & Caspers (1964), Little & Casciani (1966), van der Lugt, Smit & Caspers (1966), Myrberg (1968), Casciani (1969), Knoubovets (1969) and Forslind & Myrberg (1969). The majority of these papers deals with biological apatites.

The experiments presented in this paper form part of a systematic investigation of mineral apatites by means of n.m.r. Previous publications in this field refer to n.m.r. of fluorine in fluorapatite and of hydrogen in hydroxyapatite (van der Lugt & Caspers, 1964; van der Lugt, Smit & Caspers, 1966). The results of these two investigations are almost the same and they are briefly reviewed below.

(1) If the external field $\mathbf{H}_0$ is parallel to the *c* axis the line shape is a poorly resolved triplet (Fig. 1). This shape is characteristic of an infinite linear chain of magnetic moments with spin $\frac{1}{2}$ coupled by dipolar interaction. Experimentally, it is found that the distance Δ between the satellites is 3·64 Oe for fluorine in fluorapatite and 3·74 Oe for protons in hydroxyapatite. It can be shown that for a quantitative approach to the line-shape problem only dipolar interactions between nuclei in the same chain need to be considered. The experimental values of Δ are in satisfactory agreement with those derived from a theoretical approach in which the theory of moments (van Vleck, 1948) is applied to an infinite linear chain.

(2) A large anisotropy of the line shape is expected if $\mathbf{H}_0$ is turned away from the *c* axis. This has been confirmed experimentally. The second moment of the line is in good approximation, proportional to $(3\cos^2\theta - 1)^2$, where θ is the angle between $\mathbf{H}_0$ and the *c* axis.

The hydroxyapatite crystal used for the measurements mentioned above was rather small. For the present investigation, a larger crystal was available from a deposit in Holly Springs (Georgia, U.S.A.), its weight being 1·34 grams. As expected, when the measurements were repeated with this crystal a higher signal-to-noise ratio was obtained. In the Holly Springs mineral samples approximately 1 out of 12 hydroxyl groups is replaced by a fluorine ion (Kay, Young & Posner, 1964; Sudarsanan & Young, 1969). They are, therefore, very suitable for a more detailed investigation of the fluorine in fluoride-contaminated hydroxyapatite.

Experimental difficulties arising from the small concentration of fluoride present in the mineral sample were anticipated. Special measures had to be taken in order to obtain a usable signal-to-noise ratio. This was achieved by the application of signal-accumulation

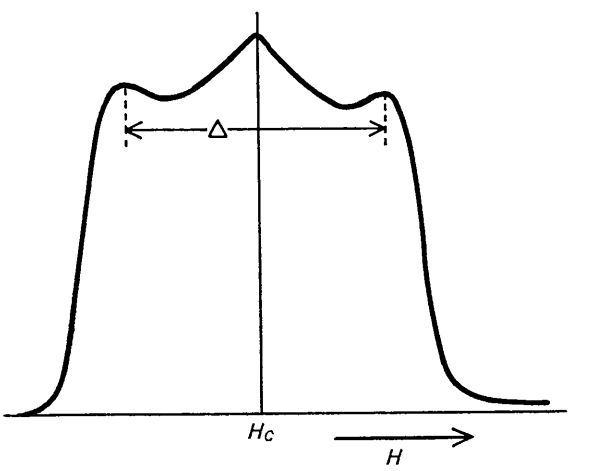

Fig. 1. Fluorine n.m.r. line in fluorapatite. The external field $\mathbf{H}_0$ is parallel to the *c* axis, Δ is 3·64 Oe.

techniques. The following investigations were carried out:

(1) a confirmation of the results previously obtained for protons in hydroxyapatite;

(2) a study of the fluorine nuclear resonance line-shape by means of signal-accumulation techniques;

(3) a more detailed study of the proton line, also by means of signal-accumulation techniques.

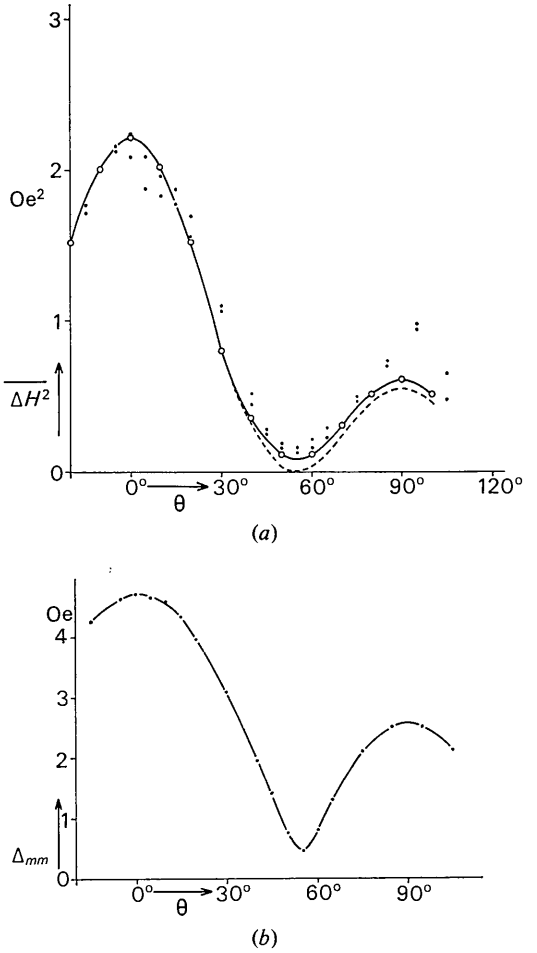

Fig. 2. (*a*) Angular dependence of the second moment of the proton line in hydroxyapatite. θ is the angle between $\mathbf{H}_0$ and the *c* axis. The second moment is independent for rotation of $\mathbf{H}_0$ about the *c* axis. For the meanings of the full and dashed curves, see the text. (*b*) Angular dependence of Δ_{mm}, the distance between maximum and minimum of the derivative of the absorption line, for protons in hydroxyapatite.

Experimental

For the proton measurements a Varian V4311 spectrometer was used. The magnetic field was calibrated by modulating the resonance frequency field with 4258 Hz and recording the proton resonance of a water sample. In this way several resonance lines separated by 1 Oe were produced. For further technical details see a previous communication (van der Lugt, Smit & Caspers, 1966).

The fluorine measurements were carried out with a Varian VF16 spectrometer, tuned at 15 MHz. The magnetic field was supplied by a Varian V3603 rotatable magnet controlled by a Mark II Fieldial. Long term stability of the field ($\pm$ 100 mOe in 24 hours) was essential for the practical feasibility of the fluorine resonance experiments.

In order to obtain a satisfactory signal-to-noise ratio, the lock-in amplifier, which forms part of the Varian wide line system, was connected to a computer of average transients (CAT 900). The signal was periodically scanned with a scanning time of about 4½ min using the saw-tooth mode of the field control unit. Between two scans the voltage over the retransmitting potentiometer changes suddenly. This step function is transformed into a pulse which starts a sampling cycle of the 'CAT'. The address advance is triggered by pulses derived from a stable audio frequency generator. Its frequency is adjusted in order to make the time needed to scan the 1024 addresses of the 'CAT' a fraction smaller than the field scanning time. The magnetic field was calibrated by superimposing proton resonance signals, recorded at different frequencies, in the memory of the 'CAT'.

The probe holder described by van der Lugt, Smit & Perdok (1968) was used to determine the orientation of the crystal. The accuracy obtained was estimated to be $\pm 1°$.

Results

Proton line, preliminary results

Fig. 2(*a*) shows the anisotropy of the second moment

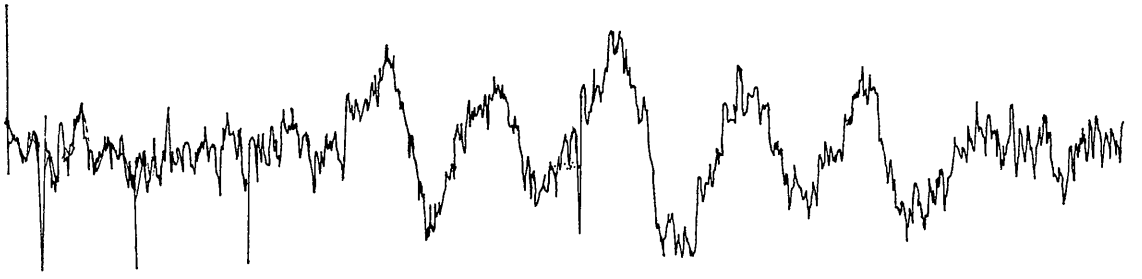

Fig. 3. Recording of the first derivative of the fluorine n.m.r. absorption line for fluorine as impurity in hydroxyapatite. $\mathbf{H}_0$ is parallel to the *c* axis.

of the proton line in hydroxyapatite. For comparison, second moments calculated according to van Vleck's formulae have been added. The full line represents second moments calculated by taking into account contributions from 125 unit cells. Contributions from the remaining part of the lattice could be neglected. The dashed line represents second moments calculated for isolated chains. For this case, the second moment is proportional to $(3\cos^2\theta-1)^2$. Fig. 2(*b*) shows the angular dependence of the line width Δ_{mm}, the distance between maximum and minimum of the derivative of the absorption line.

The line shape for $\mathbf{H}_0 \parallel c$-axis is practically the same as the fluorine line shape given in Fig. 1 and is therefore not reproduced here. The value of Δ is slightly larger than that for fluorine in fluorapatite, in accordance with the larger magnetic moment of the proton. For further details see van der Lugt, Smit & Caspers (1966).

Fluorine line

Four recordings were made of the fluorine resonance line for $\mathbf{H}_0 \parallel c$-axis. Fig. 3 shows a representative example obtained by signal accumulation for 24 hours. The integrated curve is shown in Fig. 4. It consists of five well separated components whose intensity ratios are approximately 1:1:2:1:1. Note that the components are much better resolved than the components of the triplet found for fluorine in fluorapatite and for protons in hydroxyapatite. Moreover, the separations are larger.

Anticipating the physical interpretation of the results, we consider the line as being a superposition of a triplet and a doublet. The triplet consists of the central component and the two outer components, while the remaining two components are ascribed to the doublet. The distance, in field units, between the two outer components of the triplet is $10{\cdot}74 \pm 0{\cdot}20$ Oe and the distance between the components of the doublet is $5{\cdot}98 \pm 0{\cdot}24$ Oe.

Fig. 5 shows the triplet and doublet splittings as a function of the angle θ between $\mathbf{H}_0$ and the c axis. The points represent the distance of each component from the centre of the line. The curves in Fig. 5 are of the form $A(3\cos^2\theta-1)$. The values of A were chosen so as to provide the best fit to the three highest points of the curve ($\theta=-10$, 0 and 10°). These were $A=2{\cdot}72\pm 0{\cdot}11$ Oe for the triplet and $A=1{\cdot}49\pm 0{\cdot}10$ Oe for the doublet, in agreement with the four measurements at $\theta=0°$ within the quoted limits of accuracy.

From geometrical considerations it may be said that a component is seemingly shifted from its true position towards an adjacent component if the distance between the two components becomes so small that they are not well separated. Accordingly, the fit of the experimental curves to the curves representing $A(3\cos^2\theta-1)$ is satisfactory.

Between $\theta=40$ and $\theta=60°$ the intensity of the line becomes so small that it is almost unobservable. An attempt was made to explain the disappearance in terms of a poor spin-lattice relaxation. Indeed, a narrow line can be saturated more easily than a broad line, but this alone is not sufficient to explain the effect. Assuming that the motion of neighbouring protons is responsible for the spin-lattice relaxation, an attempt has been made to calculate the anisotropy of the spin-lattice relaxation time. The results of Kay, Young & Posner (1964) concerning the motion of the hydroxyl groups were used; however, these attempts were not successful.

Experimental sources of error are: noise, magnetic-field drift, modulation width, saturation and instability of the pulse generator triggering the address advance of the 'CAT'. The short-term field drift is negligible and the long-term drift produces only a slight broadening of the components. Some saturation could not be avoided but its influence was shown to be negligible. The stability of the pulse generator was checked and found to be adequate. The only possible source of systematic error remaining is the modulation width, a rather large value of which had to be chosen (1 Oe for $\theta=90°$). This would affect the experimentally obtained separation between the components only if the components are not symmetric in shape. More particularly it might enhance the tendency of the doublet components to 'climb on the slope' of the central component.

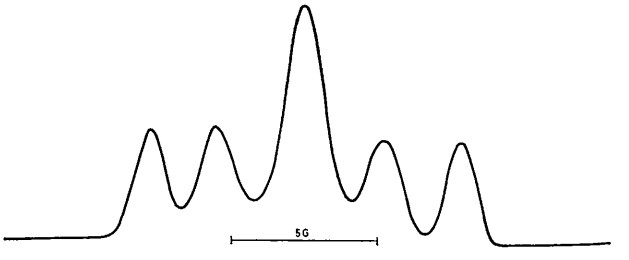

Fig. 4. Absorption line of fluorine in hydroxyapatite, obtained by integration from Fig. 3.

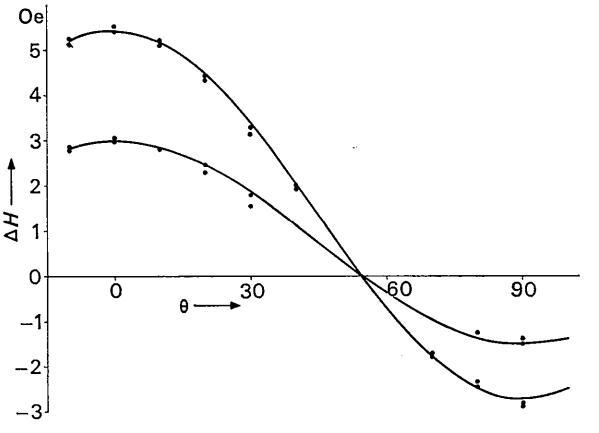

Fig. 5. Angular dependence of the outer and inner satellite components of the absorption line of fluorine in hydroxyapatite. ΔH is the shift relative to the undisplaced central line, in Oe. Full lines represent $2{\cdot}72\ (3\cos^2\theta-1)$ and $1{\cdot}49\ (3\cos^2\theta-1)$ Oe, where θ is the angle between $\mathbf{H}_0$ and the c axis.

The experimental result that the doublet splitting is slightly larger than half the triplet splitting is thus real and not due to experimental errors.

Proton line, recorded with the 'CAT'

Fig. 6(*a*) and (*b*) are photographs of the oscilloscope screen of the 'CAT' displaying the proton signal obtained by long term (12 hours) accumulation.* In two respects this curve (the derivative of the absorption curve for $\theta=0°$) differs from the one mentioned by van der Lugt, Smit & Caspers (1966).

First, there is a small hump at either side of the main part of the resonance line. These can be interpreted as being the left- and right-hand parts of the derivatives of two small additional absorption peaks with a mutual separation of 6·5–7·0 Oe.

Second the 'shoulders' (satellite peaks) of the main absorption line, produced by integration of the curves of Fig. 6(*a*) and (*b*) are not as clearly resolved as, for example, those of the fluorine absorption curve or the proton line in the paper of van der Lugt, Smit & Caspers (1966). An unambiguous explanation of this discrepancy has not been found. It may perhaps be due to a small amount of proton contamination of the probe head, which has sometimes been observed (and which is certainly not responsible for the small humps mentioned in the foregoing paragraph).

* Due to a temporary defect in the 'CAT' memory, the paper recordings were not suitable for reproduction.

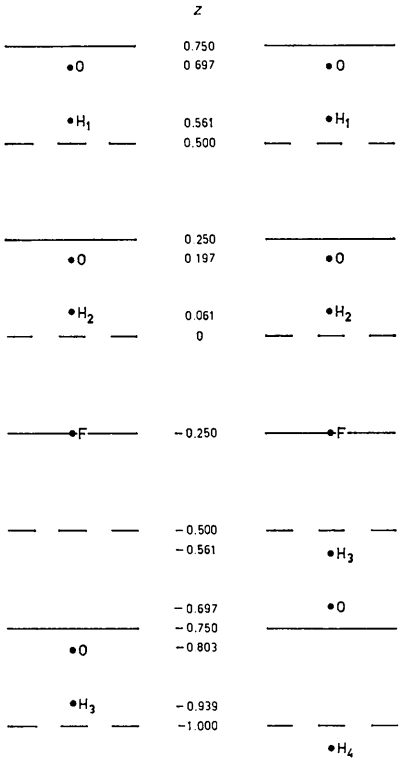

Fig. 7. Model of the interrupted chain. The *c* axis lies vertically in the plane of the paper. Full lines represent the mirror planes through the Ca^{2+} triangles as found in pure fluorapatite. The numbers are *z* axis parameters. Left the OH–F–vacancy configuration, right the OH–F–HO configuration.

Analysis

The splitting of the fluorine line is discussed in terms of nuclear dipole–dipole interactions. The experimental observation that the line consists of a limited number of well separated components suggests that we can restrict our attention to dipolar interactions within a small group of nuclei isolated from the remaining part of the crystal. In principle, the n.m.r. results alone do not allow us to specify unambiguously the number, type and location of the nuclei participating in such a group. But if the X-ray and neutron diffraction results (Kay, Young & Posner, 1964; Sudarsanan & Young, 1969) and the infrared data (Young, van der Lugt & Elliott, 1969; Fowler, 1968) are also considered, the model proposed below seems to be the only satisfactory one. The following observations were noted in finding the proposed configurations.

(1) From the measured line shapes it follows that the $\cdots$F–F–F$\cdots$ chains occurring in fluorapatite are absent in hydroxyapatite. These chains should give rise to the satellite peaks at distances of about $\pm 1{\cdot}8$ Oe from the centre of the line. Noise and the large modulation amplitude used may obscure weak satellite peaks. As a rough estimate, we can say that less than 10% of the F atoms occur in the linear arrays of the type found for F in fluorapatite.

(2) The separation of the components is much larger than found for F in fluorapatite and for H in hydroxyapatite. The magnitude of the splitting leaves practically only F and H as possible partners for the interaction with the fluorine nuclei. Indeed, the possibility of F–P interactions with an F^- ion substituted for phosphate group O^{2-} ion can not be definitely excluded by this argument, but it is ruled out by symmetry considerations (see observation 3, below).

(3) The splitting is proportional to $(3\cos^2\theta-1)$, where θ is the angle between $\mathbf{H}_0$ and the **c** direction. This suggests that the lines connecting the fluorine nuclei and the nuclei that contribute to the splitting are parallel to the *c* axis.

Based on observations (1), (2) and (3) and the diffraction and infrared data, the following model is proposed.

The fluoride ions occur in linear arrays H–F–H and H–F–vacancy parallel to the *c* axis. This is illustrated in Fig. 7. The H–F–H configuration gives rise to the triplet, the H–F–vacancy configuration gives rise to the doublet. By this assignment the observed number of components is explained ($i=\frac{1}{2}$ for F- and H-nuclei). According to the measured intensities of the components the number of fluorine nuclei in the H–F–H configuration approximates twice the number of fluorine nuclei in the H–F–vacancy configuration.

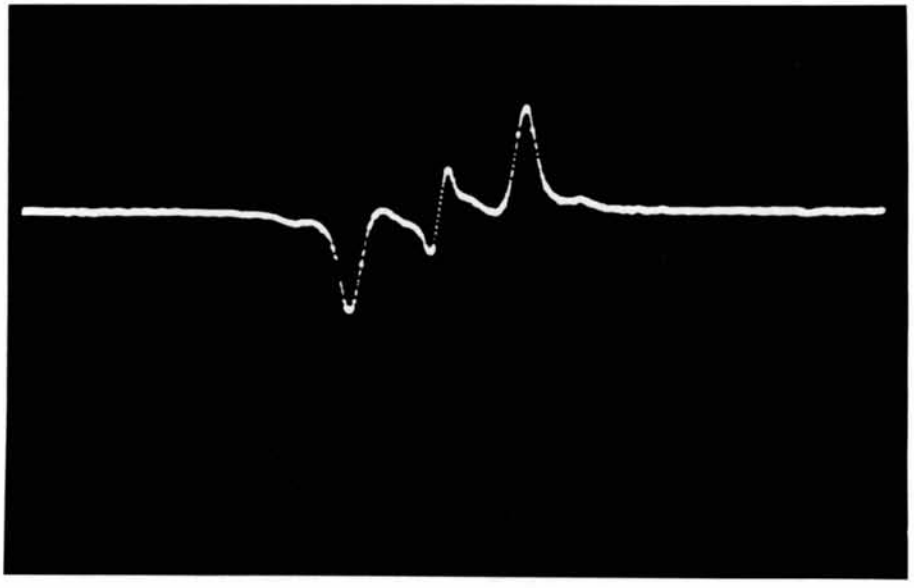

(*a*)

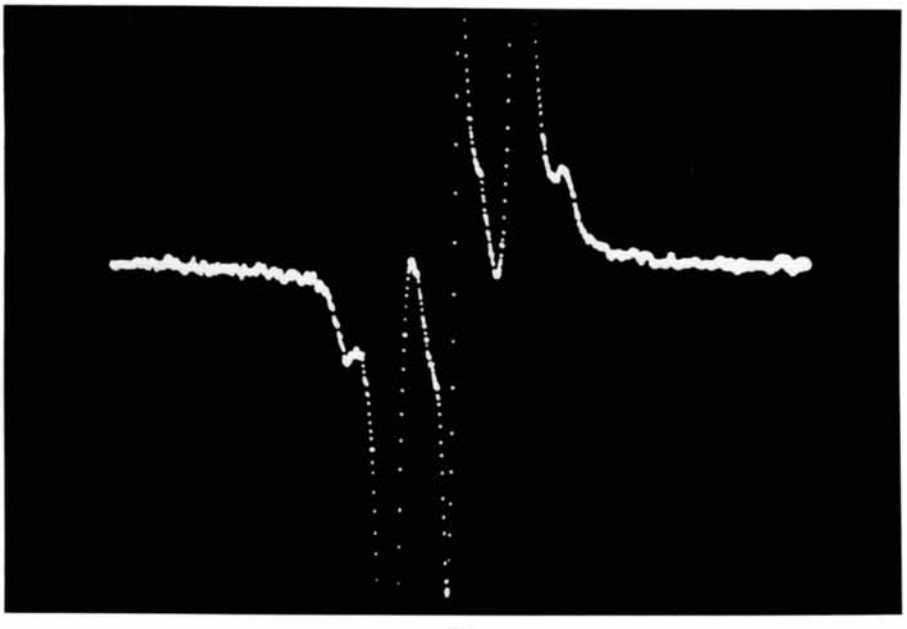

(*b*)

Fig. 6. (*a*) Derivative of the proton absorption line displayed on the oscilloscope screen of the 'CAT'; (*b*) as (*a*), but with the *y*-sensitivity increased tenfold.

For a quantitative treatment both the H–F–vacancy and the H–F–H configurations are considered as isolated groups, *i.e.* dipolar interactions with magnetic moments outside the group are neglected. This is justified below.

The splitting of the fluorine line in the H–F–vacancy configuration is given by

$$\triangle H = \pm \tfrac{1}{2}\gamma_p \hbar a^{-3}(3\cos^2\theta - 1)\,, \qquad (1)$$

where $\triangle H$ is the distance, expressed in magnetic field units, of each component from the line centre; a is the distance between a fluorine and a hydrogen nucleus, and θ is the angle between $\mathbf{H}_0$ and the line connecting the two nuclei.

The splitting of the fluorine line in the H–F–H configuration constitutes a slightly more complicated problem. We give a short derivation of the energy level scheme for the H–F–H configuration, first for an asymmetric configuration (unequal H–F distances), then, by specialization, for the symmetric configuration.

The secular part of the perturbation Hamiltonian operator is

$$\mathscr{H}_1 = A\{I_{1z}I_{2z} - \tfrac{1}{4}[I_1^+ I_2^- + I_1^- I_2^+]\} + BI_{1z}I_{3z} + CI_{2z}I_{3z} \qquad (2)$$

where

$$A = (\gamma_p^2\hbar^2/r_{12}^3)\,(1-3\cos^2\theta)\,,$$
$$B = (\gamma_p\gamma_F\hbar_2/r_{13}^3)\,(1-3\cos^2\theta)$$

and

$$C = (\gamma_p\gamma_F\hbar^2/r_{23}^3)\,(1-3\cos^2\theta)\,;$$

γ_p and γ_F are the gyromagnetic ratios for the protons and fluorine nuclei respectively. The protons are labelled by indices 1 and 2, the fluorine nuclei by the index 3. I_z, $I^+ = I_x + iI_y$, $I^- = I_x - iI_y$ are the well known nuclear spin operators. The unperturbed Zeeman states are $|+++\rangle$, $|++-\rangle$, $|+-+\rangle$, $|-++\rangle$, $|+--\rangle$, $|-+-\rangle$, $|--+\rangle$ and $|---\rangle$, where the first two symbols in each ket refer to the protons 1 and 2, and the last to the fluorine nucleus. For the non-degenerate levels the diagonal matrix elements are given in Fig. 8 under the heading 'Energy shift'. The degenerate level corresponding to the states $|+-+\rangle$ and $|-++\rangle$ gives rise to the submatrix:

	$\|+-+\rangle$	$\|-++\rangle$
$\langle+-+\|$	$\frac{1}{4}(-A+B-C)$	$-\frac{1}{4}A$
$\langle-++\|$	$-\frac{1}{4}A$	$\frac{1}{4}(-A-B+C)$

Solving the secular problem we find two levels 1 and 2 with energy shifts:

$$\triangle E_1 = -\tfrac{1}{4}A + \tfrac{1}{4}\sqrt{[A^2+(B-C)^2]} \qquad (3a)$$

and

$$\triangle E_2 = -\tfrac{1}{4}A - \tfrac{1}{4}\sqrt{[A^2+(B-C)^2]}\,. \qquad (3b)$$

The corresponding eigenfunctions are

$$\psi_1 = c_{11}|+-+\rangle + c_{12}|-++\rangle \qquad (4a)$$

and

$$\psi_2 = c'_{11}|+-+\rangle + c'_{12}|-++\rangle \qquad (4b)$$

with

$$c_{11} = \alpha A, \qquad c_{12} = \alpha\{(B-C) - \sqrt{A^2+(B-C)^2}\} \qquad (4c)$$

or

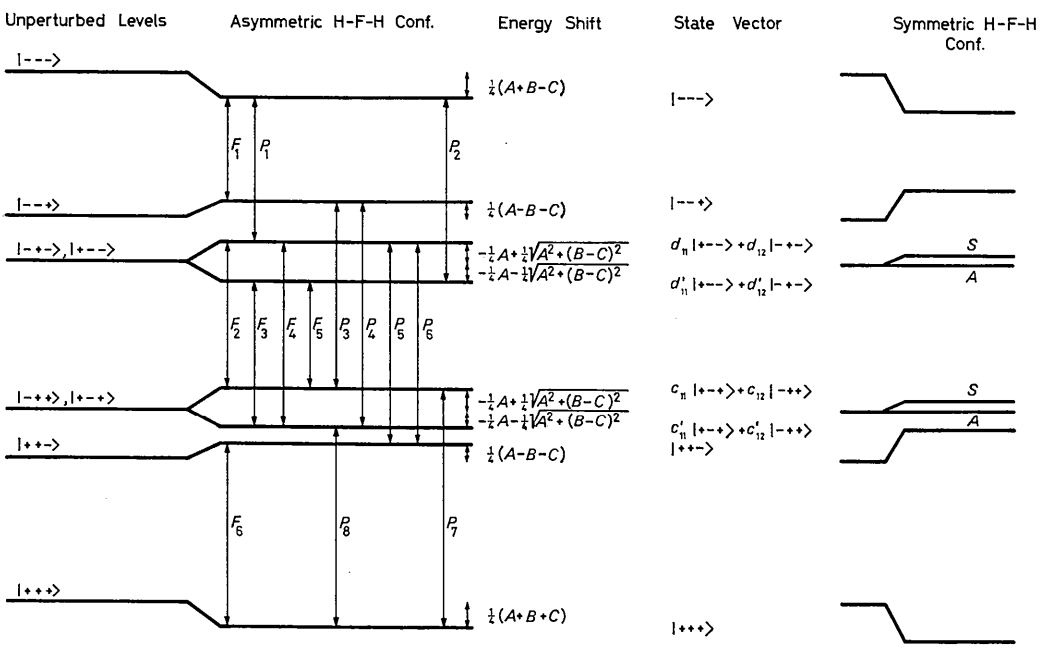

Fig. 8. Energy-level scheme for the asymmetric and symmetric H–F–H configurations. Fluorine and proton transitions are labelled F and P respectively. Energy shifts and state vectors pertain to the asymmetric configuration with $\theta = 0$ (A, B and C negative). Energy shifts and allowed transitions for the symmetric configuration are obtained by putting $B = C$. Errata: P_6 should point to the lower level originating from the state $|-+-\rangle$, $|+--\rangle$. The energy shift for the state $|---\rangle$ should read $\frac{1}{4}(A+B+C)$.

$$c_{11}=-\beta\{(B-C)+\sqrt{[A^2+(B-C)^2]}\}\,, \quad c_{12}=\beta A \qquad (4d)$$

and

$$c'_{11}=c_{12}\,, \qquad c'_{12}=-c_{11} \qquad (4e)$$

$$1/\alpha^2=2\{A^2+(B-C)^2-(B-C)\sqrt{[A^2+(B-C)^2]}\} \qquad (4f)$$

$$1/\beta^2=2\{A^2+(B-C)^2+(B-C)\sqrt{[A^2+(B-C)^2]}\}\,. \qquad (4g)$$

The expressions (4*c*) and (4*d*) for c_{11} and c_{12} are in fact identical. Note that the expressions given for the energies and coefficients of the two states are interchanged if A changes sign.

In the same way, we find two energy shifts $\triangle E_3=\triangle E_1$ and $\triangle E_4=\triangle E_2$ for the degenerate level corresponding to the states $|+--\rangle$ and $|-+-\rangle$. Writing the corresponding electron state vectors as $\psi_3=d_{11}|+--\rangle+d_{12}|-+-\rangle$ and $\psi_4=d'_{11}|+--\rangle+d'_{12}|-+-\rangle$ we find $d_{11}=c_{12}$, $d_{12}=c_{11}$, $d'_{11}=c_{11}$ and $d'_{12}=-c_{12}$.

The transitions and their relative intensities are listed in Table 1. They can also be derived from a paper by Waugh, Humphrey & Yost (1953) if one excludes a few printing errors. The position of the proton lines with the largest splitting, expressed as a magnetic field, is given by

$$H=H_0\pm\gamma_p^{-1}\hbar^{-1}(|A|+\sqrt{[A^2+(B-C)^2]})\,. \qquad (5)$$

In the specialized case ($H_1F=H_2F$) the protons occur symmetrically in the perturbation Hamiltonian operator. The correct formulae are obtained by putting $B=C$. The levels originating from each of the degenerate Zeeman levels now correspond to a symmetric and an antisymmetric state, the latter with zero-energy shift. The fluorine transitions F_4 and F_5, and the even-numbered proton lines, become forbidden. The transitions F_2 and F_3 are not shifted and contribute to the central component of the fluorine line. F_1 and F_6 correspond with the outer components of the fluorine line in the symmetric H–F–H case. For their positions we find, in magnetic field units,

$$H=H_0\pm(\gamma_p\hbar/b^3)\,(3\cos^2\theta-1)\,. \qquad (6)$$

Substituting the experimental values of the fluorine line splitting in formulae (1) and (6) we find for the H–F distance in the H–F–vacancy configuration: $a=2{\cdot}12\pm0{\cdot}03$ Å and for the H–F distance in the H–F–H configuration: $b=2{\cdot}18\pm0{\cdot}012$ Å.

It is interesting to compare these results with X-ray and neutron diffraction data obtained by Sudarsanan & Young (1969). They found, up to the third decimal, 0·197 and 0·061 for the z coordinates of the oxygen and hydrogen atom respectively in the linear chains of hydroxyapatite. On the other hand, the z coordinate of fluorine in fluorapatite is $\pm0{\cdot}250$ (Náray-Szabó, 1930). If we adopt the same value for fluorine in hydroxyapatite we find an H–F distance of 2·14 Å, in excellent agreement with the n.m.r. results. Note that the distance in the H–F–vacancy configuration is slightly smaller than that in the H–F–H configuration. This is explained by the existence of a weak hydrogen bond between the oxygen ion and the fluorine ion. The O–F distance is 3·06 Å which is long compared with the O–H–F hydrogen-bond distances mentioned by Hamilton & Ibers (1968). We may expect that a weak hydrogen bond is formed that contributes to the energy of the lattice. The preference of the fluorine ions to occupy positions in one of the two configurations might be partly due to the possibility of forming a weak hydrogen bond. More particularly the absence of fluorine ions clustering along the chain can be explained in this way.

The proposed model justifies our treatment of the H–F–vacancy and H–F–H groups as isolated groups. The strength of the dipolar interaction D between two nuclei is inversely proportional to the third power of their separation. For the following estimation of interaction strengths the interaction is multiplied by a factor 3/2 in the case of identical nuclei. The following ratios are found for the interactions within the H–F–H configuration (see Fig. 7):

$$D_{H_2F}/D_{H_1H_2}=2{\cdot}8 \qquad D_{H_2F}/D_{H_1F}=17{\cdot}7$$

and for the H–F–vacancy configuration:

$$D_{H_2F}/D_{H_1H_2}=2{\cdot}8 \qquad D_{H_2F}/D_{H_1F}=17{\cdot}7$$
$$D_{H_2F}/D_{H_3F}=10{\cdot}8\,.$$

The presence of one proton at a relatively large distance from the H–F–vacancy or H–F–H configuration causes each of the components to split. Evidently this splitting is masked by various broadening mechanisms. The secular part of the interaction between this proton and the fluorine nucleus contains only z components of the angular momenta. By the application of similar arguments, as applied by Holcomb & Pedersen (1963), it is possible to show that this broadening will be symmetric.

Table 1. *Transitions, energy shifts and relative intensities of the* H–F–H*-system for negative A, B and C*
$Q=A^2+(B-C)^2$

Transition	Energy shift	Relative transition probability	Transition	Energy shift	Relative transition probability
F_1	$\frac{1}{2}(B+C)$	1	P_1	$\frac{1}{4}(2A+B+C-\sqrt{Q})$	$(c_{11}+c_{12})^2$
F_2	0	$4(c_{11}c_{12})^2$	P_2	$\frac{1}{4}(2A+B+C+\sqrt{Q})$	$(c_{11}-c_{12})^2$
F_3	0	$4(c_{11}c_{12})^2$	P_3	$\frac{1}{4}(2A-B-C-\sqrt{Q})$	$(c_{11}+c_{12})^2$
F_4	$\frac{1}{2}\sqrt{Q}$	$(c_{11}^2-c_{12}^2)^2$	P_4	$\frac{1}{4}(2A-B-C+\sqrt{Q})$	$(c_{11}-c_{12})^2$
F_5	$-\frac{1}{2}\sqrt{Q}$	$(c_{11}^2-c_{12}^2)^2$	P_5	$\frac{1}{4}(-2A+B+C+\sqrt{Q})$	$(c_{11}+c_{12})^2$
F_6	$-\frac{1}{2}(A+B)$	1	P_6	$\frac{1}{4}(-2A+B+C-\sqrt{Q})$	$(c_{11}-c_{12})^2$
			P_7	$\frac{1}{4}(-2A-B-C+\sqrt{Q})$	$(c_{11}+c_{12})^2$
			P_8	$\frac{1}{4}(-2A-B-C-\sqrt{Q})$	$(c_{11}-c_{12})^2$

The conclusions drawn from the splitting of the fluorine line are confirmed by the proton measurements if we assume that the two side humps originate from protons being adjacent to fluorine ions. We can roughly represent the situation of such a proton as being the central nucleus of an H–H–F configuration. Then the formulae for the general case of the H–F–H problem apply. Substituting $r_{12}=3{\cdot}44$, $r_{23}=2{\cdot}15$ Å (the mean value for the H–F–H and the H–F–vacancy configuration) and $r_{13}=5{\cdot}59$ Å, the separation of the lines with the largest splitting P_1 and P_7 is found to be 6·8 Oe, in accordance with the experimental results.

The paragraphs below are devoted to some criticism of the proposed model.

One expects the intensity ratio of the central peak and the two outer peaks to be 2:1. In fact a different, usually larger, ratio is found. The deviations are about 10% if the ratio of the peak heights is considered, but may increase up to 50% if estimated areas of the components are used as measures of the intensities. This leaves open the possibility that magnetically isolated fluorine ions are present in the lattice. On the other hand, the determination of intensities from absorption curves such as the one given in Fig. 3 is subject to many possible errors, and one should proceed with caution in drawing conclusions from the discrepancy.

The same reservation applies to the interpretation of the intensity ratio of the outer components of the triplet and the components of the doublet. We find $0{\cdot}94 \pm 0{\cdot}05$ for the ratio of the heights and $0{\cdot}84 \pm 0{\cdot}05$ for the ratio of the areas. From these intensity ratios it should follow that the probability that a fluorine ion will occur in the H–F–H configuration is 1·7–1·8 times the probability that it will occur in the H–F–vacancy configuration.

Another problem to be investigated is how far the assumed parallelism of the H–F bonds and the c axis is required by the measurements. For this purpose the position of the outer components of the resonance line was calculated as a function of θ for a set of hypothetical H–F–H bonds related by sixfold rotation symmetry and all making an angle α with the c axis. Gaussian lines centred at each of these positions and of a suitable width were superimposed. The shapes and positions of the lines constructed in this way were compared with the experimentally obtained components. It was found that $\alpha=10°$ was still permitted by the experiments, but $\alpha=20°$ was excluded. Only straight H–F–H configurations were considered.

The authors gratefully acknowledge the contributions of the following persons and institutions. Professor R. A. Young (Georgia Institute of Technology, Atlanta, U.S.A.) not only made available the Holly Springs mineral crystal but also his wide knowledge of apatite structures. Dr J. C. Elliott gave a preliminary report of spectroscopic investigations. Mr W. H. M. Koopman undertook part of the proton measurements. Mr J. Broeze constructed the electronic equipment for controlling the 'CAT'. The line splitting problem was solved in close cooperation with Dr H. P. van de Braak. Dr J. R. Luyten (Computer Center of the University) wrote a computer program for the superposition of Gaussian lines mentioned in the last section. The physical chemistry department of the University provided technical facilities and gave valuable advice.

This work is part of the research programme of the Stichting voor Fundamenteel Onderzoek der Materie (F.O.M.), and has been made possible by financial support from the Nederlandse Organisatie voor Zuiver Wetenschappelijk Onderzoek (Z.W.O.).

References

Bhatnagar, V. M. (1969). *Contr. Miner. Petrol.* **22**, 375
Boer, T. H. de (1957). Thesis, Groningen.
Casciani, F. S. (1969). Communication at the Second International Symposium on the Composition, Properties and Fundamental Structure of Tooth Enamel, the London Hospital Medical College, 16th and 17th June, 1969.
Elliott, J. C. (1969). *Calc. Tiss. Res.* **3**, 293.
Forslind, E. & Myrberg, N. (1969). Communication at the ORCA (European Organization for Caries Research) Congress, Stockholm, 1–3 July, 1969; to be published in *Caries Research*.
Fowler, B. O. (1968). International Symposium on Structural Properties of Hydroxyapatite and Related Compounds, NBS, Gaithersburg, Maryland, USA, 12–14 September.
Hamilton, W. C. & Ibers, J. A. (1968). *Hydrogen Bonding in Solids*. New York, Amsterdam: Benjamin.
Hayashi, S. (1960). *Nippon Kagaku Zasshi*, **81**, 540.
Hentschel, H. (1923). *Central. Miner. Geol.* p. 609.
Holcomb, D. F. & Pedersen, B. (1963). *J. Chem. Phys.* **38**, 54.
Kay, M. I., Young, R. A. & Posner, A. S. (1964). *Nature, Lond.* **204**, 1050.
Knoubovets, R. G. (1969) *Spectroscopy Letters*, 2, 121
Little, M. F. & Casciani, F. S. (1966). *Archs. oral. Biol.* **11**, 565.
Lugt, W. van der & Caspers, W. J. (1964). *Physica*, **30**, 1658.
Lugt, W. van der, Smit, W. A. & Caspers, W. J. (1966). Proc. XIVth Colloque Ampère, Ljubljana. Ed. R. Blinc.
Lugt, W. van der, Smit, W. A. & Perdok, W. G. (1968). *Acta Cryst.* A**24**, 439.
Mehmel, M. (1930). *Z. Kristallogr.* **75**, 323.
Myers, H. M. (1965*a*). *Nature, Lond.* **206**, 713.
Myers, H. M. (1965*b*). *Expl. Cell. Res.* **38**, 686.
Myrberg, N. (1968). Thesis, Transactions of the Royal Schools of Dentistry, Umeå, Sweden.
Náray-Szabó, S. (1930). *Z. Kristallogr.* **75**, 387.
Structure Reports (1952). **16**, 329. Utrecht: Oosthoek.
Structure Reports (1953). **17**, 492. Utrecht: Oosthoek.
Structure Reports (1956). **20**, 309. Utrecht: Oosthoek.
Sudarsanan, K. & Young, R. A. (1969). *Acta Cryst.* B**25**, 1534.
Vleck, J. H. van. (1948). *Phys. Rev.* **74**, 1168.
Waugh, J. S., Humphrey, F. B. & Yost, D. M. (1953). *J. Phys. Chem.* **57**, 486.
Young, R. A. & Elliott, J. C. (1966). *Arch. oral. Biol.* **11**, 699.
Young, R. A., van der Lugt, W. & Elliott, J. C. (1969). *Nature, Lond.* **223**, 729.